JACS
JOURNAL OF THE AMERICAN CHEMICAL SOCIETY
pubs.acs.org/JACS
Article

On-Surface Design of a 2D Cobalt-Organic Network Preserving Large Orbital Magnetic Moment

Cristina Martín-Fuentes,[○] Sofia O. Parreiras,*[,○] José I. Urgel, Víctor Rubio-Giménez, Beatriz Muñiz Cano, Daniel Moreno, Koen Lauwaet, Manuel Valvidares, Miguel A. Valbuena, Pierluigi Gargiani, Wolfgang Kuch, Julio Camarero, José M. Gallego, Rodolfo Miranda, José I. Martínez,* Carlos Martí-Gastaldo,* and David Écija*

Cite This: *J. Am. Chem. Soc.* 2022, 144, 16034−16041
Read Online

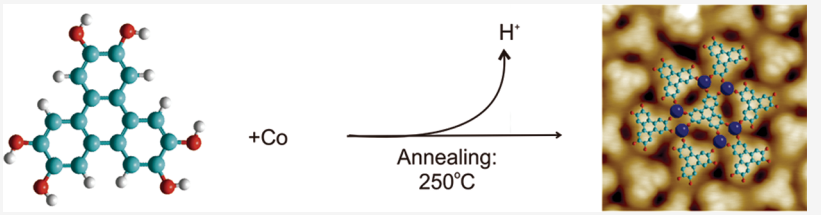

ABSTRACT: The design of antiferromagnetic nanomaterials preserving large orbital magnetic moments is important to protect their functionalities against magnetic perturbations. Here, we exploit an archetype H_6HOTP species for conductive metal−organic frameworks to design a Co-HOTP one-atom-thick metal−organic architecture on a Au(111) surface. Our multidisciplinary scanning probe microscopy, X-ray absorption spectroscopy, X-ray linear dichroism, and X-ray magnetic circular dichroism study, combined with density functional theory simulations, reveals the formation of a unique network design based on threefold Co^{+2} coordination with deprotonated ligands, which displays a large orbital magnetic moment with an orbital to effective spin moment ratio of 0.8, an in-plane easy axis of magnetization, and large magnetic anisotropy. Our simulations suggest an antiferromagnetic ground state, which is compatible with the experimental findings. Such a Co-HOTP metal−organic network exemplifies how on-surface chemistry can enable the design of field-robust antiferromagnetic materials.

INTRODUCTION

Magnetic anisotropy is a fundamental property in magnetism responsible for the preferential directions of magnetization. Atomistically, the spin−orbit coupling connects the spin and the orbital magnetic moment of a material. This, together with the orbital anisotropy, gives rise to magnetic anisotropy. According to Hund's rules, free transition metal atoms can possess large orbital magnetic moments. However, whenever such atoms are located in a solid, crystal field effects typically split the energy degeneracy of d-orbitals, which causes partial or total quenching of the orbital magnetic moment.[1] Much effort has been devoted to overcome such limitations, mostly centered on reducing the coordination of the transition metal to increase the orbital magnetic moment and, thus, enhance the magnetic anisotropy. However, these efforts have been mainly concentrated on controlling local coordination environments of discrete molecules,[1−7] whereas the route to comparable control in extended solids remains still blocked. In this regard, the design of antiferromagnetic solids is particularly relevant in spintronics because of their robustness against perturbations from magnetic fields, while not producing stray fields.[8,9] Herein, magnetic anisotropy is one of the key parameters that determine the degree of protection. The capability to preserve a large orbital magnetic moment in two-dimensional metal−organic networks[10−12] is crucial to steer spin−orbit coupling and enhance magnetic anisotropy. Large magnetic anisotropy has been theoretically predicted for some two-dimensional (2D) metal−organic systems;[13−16] however, the experimental achievement of such systems has remained elusive.

Metal−organic frameworks (MOFs) have emerged as molecule-based architectures with chemical and structural versatilities not comparable to any other synthetic material.[17] The last decade has witnessed how the synthetic control over metal nodes and organic ligands has enabled the design of materials for targeted applications in fields as diverse as sensing, gas storage/separation, catalysis, light emission, energy harvesting, or magnetism.[17−23] Chemical diversity and structural tunability have also been central tools for engineer-

Received: June 3, 2022
Published: August 25, 2022

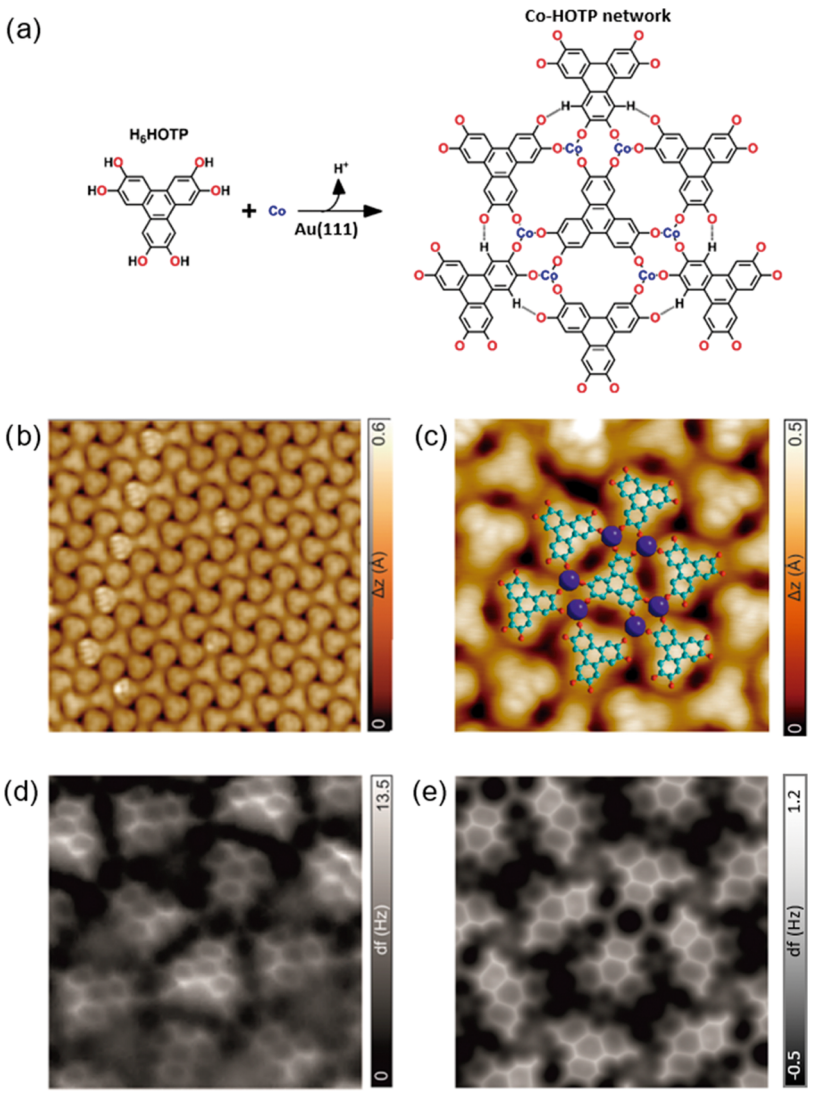

Figure 1. On-surface design of the Co-HOTP network on Au(111). (a) Synthetic route toward the design of Co-HOTP on Au(111). (b) Mid-range STM image of the coordinative architecture. (c) High-resolution STM image with a superimposed ball and stick model. Green, red, and violet spheres depict carbon, oxygen, and cobalt atoms, respectively. (d) Constant-height frequency-shift nc-AFM image acquired with a CO-functionalized tip. (e) nc-AFM simulation of (d). Image size: (b) 11.7 nm × 11.7 nm; (c) 4 nm × 4 nm; and (d, e) 3.2 nm × 3.2 nm. STM parameters: (b) V_b = 20 mV, I_t = 120 pA, and T = 4 K; (c) V_b = 20 mV, I_t = 100 pA, and T = 4 K; and (d) open feedback: V_b = 5 mV, I_t = 150 pA, Z_{offset} = 150 pm, and T = 4 K.

ing the properties of two-dimensional conjugated metal−organic frameworks (2D c-MOFs).[24] Such metal−organic nanomaterials are built from the packing of layers formed by transition metal ions coordinated to −NH_2, −OH, −SH, or −SeH functional groups with single/polyaromatic cores and predominantly crystallize in porous hexagonal honeycomb lattices, while there are only a handful of examples of dense Kagome networks with benzene- and coronene-based ligands. From a physical standpoint, chemical control of these systems can allow for the augmented mobility of charge carriers due to extended intralayer conjugation[24−26] or the expression of novel quantum phases of matter.[27−31] The possibility of confining their growth to just atomically thick 2D layers by an on-surface chemistry approach offers exciting opportunities for investigating their electronic and magnetic properties at the ultimate spatial resolution,[32−34] which now we contribute to extend to the assembly of topologies and metal coordination indexes only accessible in solvent-free environments.[35−37]

Here, we carried out a multidisciplinary study combining scanning tunneling microscopy (STM) and spectroscopy (STS), noncontact atomic force microscopy (nc-AFM), X-ray adsorption spectroscopy (XAS), X-ray linear dichroism (XLD), X-ray magnetic circular dichroism (XMCD), and density functional theory complemented by a Hubbard model (DFT + U), to illustrate the on-surface synthesis of an unprecedented Co-HOTP metal−organic network on Au(111) based on the deprotonation of H_6HOTP (2,3,6,7,10,11-hexahydroxytriphenylene) species and their subsequent coordination with cobalt (Co) atoms. The Co-HOTP architecture displays a large orbital magnetic moment with an orbital to effective spin moment ratio of 0.8, an in-plane easy axis of magnetization, and large magnetic anisotropy. Our density functional calculations predict the antiferromagnetic nature of the coordinative assembly, which agrees with the XLD/XMCD results. Thus, our findings illustrate avenues to engineer field-robust antiferromagnetic materials.

https://doi.org/10.1021/jacs.2c05894
J. Am. Chem. Soc. 2022, 144, 16034−16041

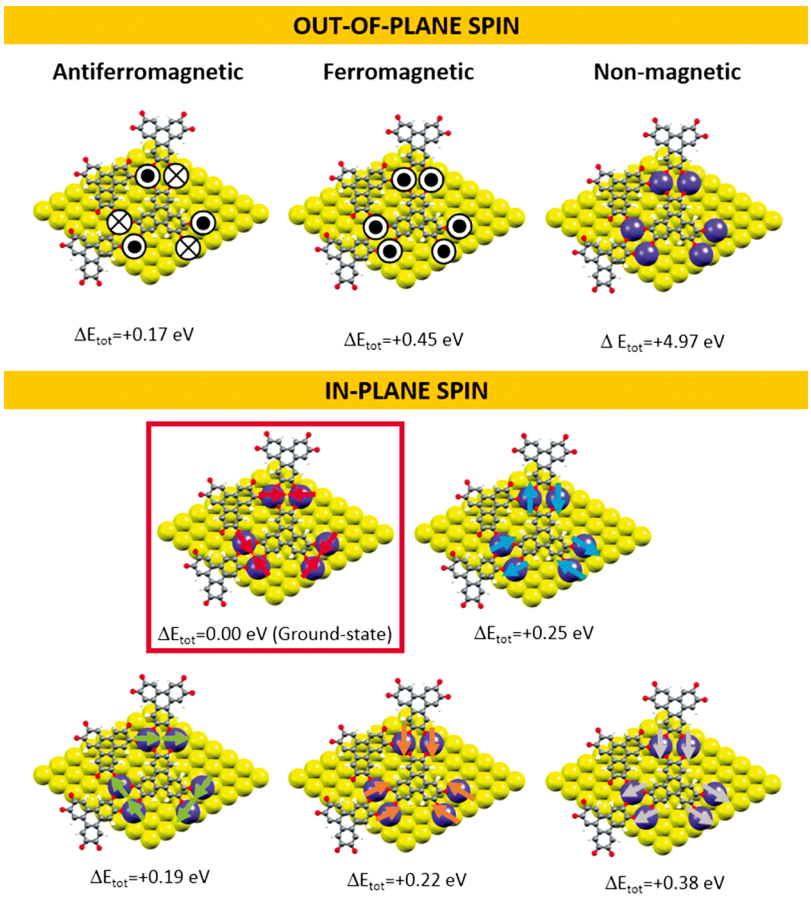

Figure 2. Schematic top view of (fully structurally and electronically relaxed) different interfacial spin configurations considered in the calculations including both the Co-HOTP network and the Au substrate to elucidate the spin ground state: (top) antiferromagnetic, ferromagnetic, and spin-unpolarized out-of-plane spin cases; and (bottom) representative inequivalent in-plane spin configurations. The red square highlights the ground state.

RESULTS AND DISCUSSION

The deposition of a submonolayer coverage of 2,3,6,7,10,11-hexahydroxytriphenylene (H_6HOTP)[38−41] (cf. left panel of Figures 1a, SI1, and SI2) on a clean Au(111) surface and further annealing to 250 °C, gives rise to a disordered self-assembled architecture coexisting with ordered patches, based on hydrogen bonds and van der Waals interactions between adjacent molecules (cf. Figure SI3).

This scenario changes in the presence of Co adatoms. The sublimation of Co on a submonolayer coverage of H_6HOTP on Au(111) held at 100 °C, and its subsequent annealing to 250 °C, results in the formation of long-range supramolecular islands with rounded borders (cf. Figure SI4). For sufficient Co dosage, no sign of the pristine H_6HOTP architecture is detected. Instead, a novel Co-directed metal−organic network is formed, to be termed Co-HOTP, thanks to the full deprotonation of the linkers[38] and the subsequent formation of Co−O bonds (cf. Figure 1a).

Such assembly is different from the previously reported 2D honeycomb $Co_3(HOTP)_2$ layers in cobalt-directed 2D c-MOFs synthesized in wet chemistry,[38] which illustrates the crucial role of surface confinement. The confinement in 2D, the interaction of the adsorbates with the surface, and the presence of high-symmetry directions direct the growth, favoring specific coordination symmetries. High-resolution STM images allow discerning two molecular orientations of the molecular species per domain, related by a 60° rotation, featuring a porous self-assembly with two distinct small pores (cf. Figure 1b,c). Notably, nc-AFM reveals the nature of the bonds (cf. Figure 1d), which are threefold Co−O links, with a mean average projected bond distance of 1.9 Å. Importantly, one species displays a fourfold coordination, whereas the other one features a sixfold coordinative scheme (see Figures SI5 and SI7), resulting in an overall periodic metal−organic architecture.

On the basis of the experimental observations, we have performed calculations based on DFT + U to obtain a fully relaxed interfacial structure. In the ground-state configuration (cf. discussion below), the molecular ligands forming the network lie flat at 3.3−3.4 Å above the Au surface, while the coordinative Co atoms are located at 2.8 and 3.2 Å above the surface. The relaxed structure yields Co−O bond lengths ranging from 1.86 to 1.92 Å, in excellent agreement with the experimental evidence from nc-AFM images (cf. Figure 1d). In addition, the simulated nc-AFM images match very well with the experimental ones, ratifying the rationalization of the self-assembly (cf. Figure 1e).

The magnetic ground state has been calculated starting from several geometrical models and spin states accounting for spin−orbit coupling and noncollinear spin effects (see further details in the Supporting Information). As illustrated in Figure 2, we have computed the energy of the following interfacial spin configurations: (i) spin-unpolarized case, (ii) ferromag-

https://doi.org/10.1021/jacs.2c05894
J. Am. Chem. Soc. 2022, 144, 16034−16041

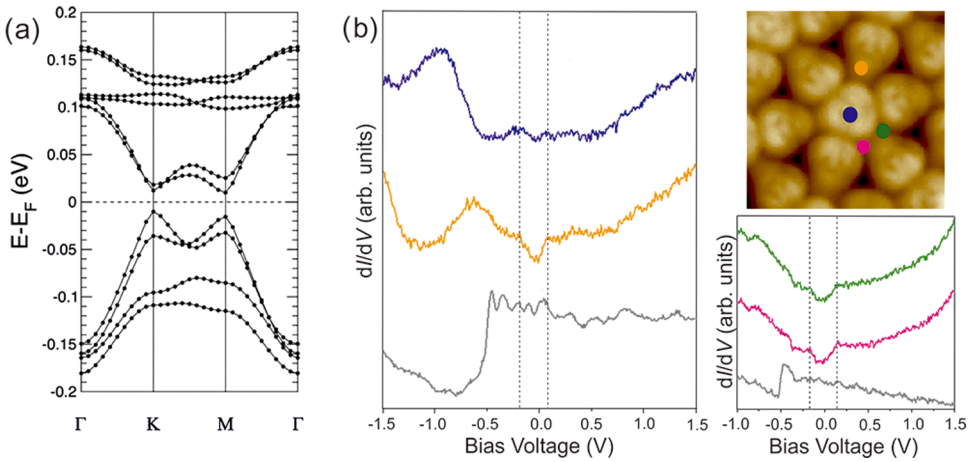

Figure 3. Electronic structure of the Co-HOTP network on Au(111). (a) Computed DFT + U (U = 3.75 eV for Co^{+2}) electronic band structure for the network ground-state spin configuration of Figure 2. The zero energy is taken to correspond to the Fermi energy, while the x-axis labels denote a path through the three-dimensional (3D) space of k-vectors. Points of high symmetry in the Brillouin zone are labeled as Γ(0,0,0), M(0,1/2,0), and K(1/3,2/3,0), all in reciprocal space coordinates. (b) dI/dV spectra on representative positions of the metal−organic network (marked with colored circles in the STM image). STS spectra acquired on clean Au(111) are depicted in gray. STM parameters: V_b = 300 mV, I_t = 300 pA, and T = 4 K. Image size: 5 nm × 5 nm.

netic and antiferromagnetic out-of-plane spin couplings, and (iii) distinct inequivalent in-plane spin cases.

Such calculations reveal that the most energetically favorable configuration for both free-standing (cf. Figure SI6) and surface-confined networks corresponds to the local noncollinear antiferromagnetic state with all spins in-plane (highlighted in Figure 2 by a red square) and with Co atoms featuring a +2 oxidation state.

We have inspected by DFT + U the electronic structure of the spin ground-state configuration (red square in Figure 2) of the interfacial network, where U has been taken in this case to be 3.75 eV, a value optimized for Co^{+2}.[42] Our results shown in Figure 3a display an electronic gap of 30 meV at the K point and band extrema at the Γ point located at −0.15 and 0.10 eV, respectively.

To experimentally probe the electronic structure of Co-HOTP, we have performed scanning tunneling spectroscopy at selected positions on the network and on Au(111). Notably, there are weak features located on the fourfold and sixfold coordinated molecular species at ∼−0.21 and ∼+0.07 eV, as well as on Co atoms at ∼−0.16 and ∼+0.13 eV (cf. Figure 3b). These features might reflect the predicted band extrema at the Γ point. The linear decrease in DOS leading to a minimum at the Fermi level might be consistent with the very small gap predicted by theory. Such a band gap is significantly smaller than the one reported in $Co_3(HOTP)_2$ frameworks.[43]

Next, we performed XAS, XMCD, and XLD measurements. Figure 4a presents XAS/XMCD spectra taken at Co $L_{2,3}$-edges at grazing (GI = 70°) and normal (NI = 0°) incidences, measured at 2 K and 6 T. The L_3-XAS spectra present a multiplet peak structure indicative of strong localization of Co 3d electrons, which is consistent with a +2 oxidation state for Co (cf. Figure SI8 and discussion in the Supporting Information),[44−47] in agreement with the results of DFT + U calculations. In addition, the XMCD signal has the same negative sign at both L_3- and L_2-edges at GI, whereas L_2 vanishes at NI; both of them are characteristic of a very large orbital moment. The XMCD is much larger at grazing incidence, i.e., a strong anisotropy with an in-plane easy axis is observed.

Table 1 displays the expectation values of effective spin ($\langle S_{eff}\rangle$) and orbital ($\langle L_z\rangle$) operators in $\hbar$ units, and effective spin ($m_{eff} = 2\langle S_{eff}\rangle$) and orbital ($m_L$) magnetic moments in μ_B, as well as the orbital to effective spin moment ratio ($\langle L_z\rangle/2\langle S_{eff}\rangle$) calculated by sum-rule analysis.[48,49] These values are actually the expectation values of the magnetic moments projected onto the X-ray incidence direction at the experimental conditions of 6 T and 2 K. Here, it is worth pointing out that the real magnetic moments can only be probed at full saturation, which is not the case (see discussion below), and, thus, in such scenarios, the expectation values of the moments represent a lower limit for the real magnetic moments.

At NI, the small magnetic dichroism reflects that the expectation values of the magnetic moments are very low. At GI, on the other side, the XMCD presents high intensity and large moments. The in-plane orbital moment is 0.98 μ_B, which is an exceptionally large and unprecedented value for a 3d metal in 2D metal−organic networks.

For the spin moment, our DFT + U calculations determine an average spin quantum number $\langle S_z\rangle$ of 0.95 for Co atoms (cf. Figure SI9 and discussion in the Supporting Information). The sum rule analysis determine the effective spin ($\langle S_{eff}\rangle = \langle S_z\rangle + 7/2\langle T_z\rangle$), whereby the dipole term ($\langle T_z\rangle$) can be significant in systems with low symmetry. In Co porphyrins, for instance, the dipole moment was found to have an inverted sign and a larger magnitude than the spin moment for some angles.[50] From the sum-rule analysis, the Co-HOTP network has an $\langle S_{eff}\rangle$ of 0.61 (6) at GI, 6 T, and 2 K. The impossibility of reaching saturation hinders the determination of the dipole term by angle-dependent measurements, so, based on the experimental data, it is not possible to unequivocally infer the spin state. Herein, it is worth noting that the real $\langle S_{eff}\rangle$ at full saturation could be larger, and the dipole term could be negative, which would bring the experimental $\langle S_z\rangle$ into agreement with the calculation.

Notably, a very large orbital to effective spin moment ratio ($\langle L_z\rangle/2\langle S_{eff}\rangle$) is observed. Such a ratio is obtained from XMCD alone and without assumptions on the number of holes, which makes it very robust with respect to background

https://doi.org/10.1021/jacs.2c05894
J. Am. Chem. Soc. 2022, 144, 16034−16041

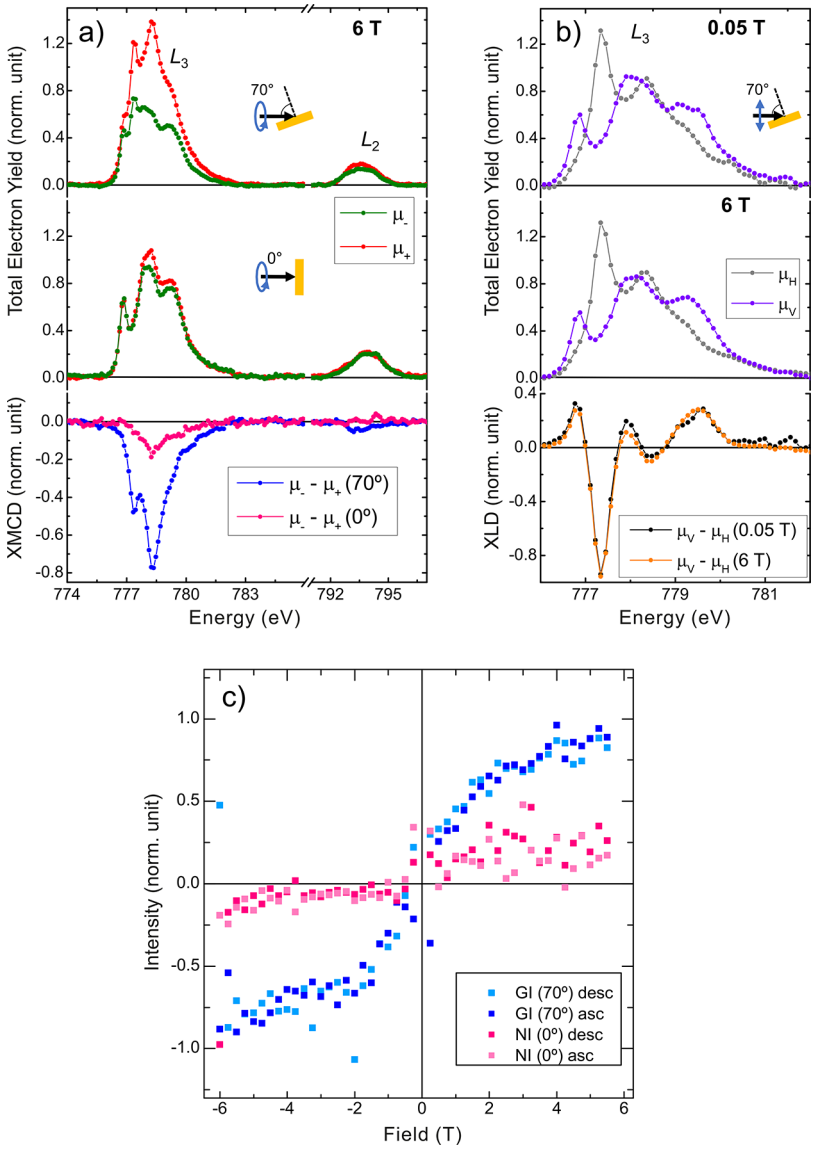

Figure 4. Magnetic properties of the Co-HOTP network on Au(111). (a) XAS spectra with positive (μ_+, red) and negative (μ_-, green) circularly polarized light and XMCD ($\mu_- - \mu_+$) taken at the Co $L_{2,3}$-edges at grazing (70°, blue) and normal (0°, pink) incidences (B = 6 T, T = 2 K). (b) XAS spectra acquired with vertical (μ_V, purple) and horizontal (μ_H, gray) linearly polarized light and XLD ($\mu_V - \mu_H$) taken at the Co L_3-edge at grazing (70°) incidence for fields of 0.05 T (black) and 6 T (orange, T = 2 K). (c) Magnetization curves constructed by measuring the XMCD intensity at the highest peak of the Co L_3-edge at grazing (70°, blue) and normal (0°, pink) incidences. Dark (light) dots represent the descending (ascending) branches (T = 2 K).

Table 1. Effective Spin ($\langle S_{eff}\rangle$) and Orbital ($\langle L_z\rangle$) Operators in $\hbar$ Units, Effective Spin ($m_{S_{eff}}$) and Orbital (m_L) Moments in μ_B, and the Orbital to Effective Spin Moment Ratio ($\langle L_z\rangle/2\langle S_{eff}\rangle$) Extracted by XMCD Sum-Rule Analysis for Grazing (70°) and Normal (0°) Incidences at 6 T and 2 K for Co Centers on the Co-HOTP Network on Au(111)

incidence angle (°)	$\langle S_{eff}\rangle$ ($\hbar$)	$\langle L_z\rangle$ ($\hbar$)	$m_{S_{eff}}$ (μ_B)	m_L (μ_B)	$\langle L_z\rangle/2\langle S_{eff}\rangle$
70	0.61 (6)	0.98 (10)	1.22 (12)	0.98 (10)	0.80 (11)
0	0.14 (1)	0.19 (2)	0.28 (3)	0.19 (2)	0.68 (10)

subtraction. Notice that this ratio is close to the ones reported in the case of 3d adatoms on top of metallic alkali surfaces.[51] The ratio of orbital to effective spin magnetic moment changes from 0.80 to 0.68 between GI and NI. Because of the unknown contribution of the dipole term, no direct conclusion about the anisotropy of the orbital moment can be drawn from these numbers. However, since the $\langle T_z\rangle$ term enters with opposite sign in the two measurements,[50] the ratio of orbital to spin moment is either in between these two values, or >0.80 for GI and <0.68 for NI. In any case, these are extraordinarily high values for transition metal coordination networks.

XLD spectra at a low magnetic field (0.05 T, see Figure 4b) feature giant anisotropy, with more than 90% of dichroism. This is an indication of strong charge density anisotropy due to the coordinative crystal field. Consequently, any possible magnetic contribution to the XLD is hidden by the charge

https://doi.org/10.1021/jacs.2c05894
J. Am. Chem. Soc. 2022, 144, 16034−16041

effect, and when a 6 T field is applied, the shape of XLD is similar, only with subtle differences in the peak's intensity.

Magnetization curves for GI and NI are shown in Figure 4c. For NI, the curve is almost linear with low intensity even at 6 T. In the case of GI, larger susceptibility and some curvature are observed. However, it is worth noting that in the case of GI also, the magnetization curve is not at saturation, possibly indicating the presence of antiferromagnetic interactions among Co moments. These results, together with the XLD/XMCD findings, are compatible with weak antiferromagnetism, as predicted by DFT + U.

CONCLUSIONS

In summary, we report the on-surface synthesis of a Co-HOTP metal−organic network on Au(111) based on the coordination of H_6HOTP species with Co upon thermal activation of -OH groups. The resulting coordinative pattern relies on fourfold and sixfold coordinative species, giving rise altogether to a unique periodic architecture, which illustrates the power of surface-confined metal−organic chemistry to design unparalleled low-dimensional architectures. A comprehensive STS study, complemented by DFT + U calculations, reveals that the network features a very low band gap. Our calculations illustrate that the coordinative architecture displays an antiferromagnetic ground state, with Co presenting a +2 oxidation state. Such findings are compatible with our XAS, XLD, and XMCD investigations. As a result of its low coordination index, cobalt atoms exhibit a large unquenched orbital magnetic moment and a large orbital to effective spin moment ratio unprecedented in 2D coordinative architectures based on 3d metals. We are confident that our results open new pathways for the engineering of antiferromagnetic low-dimensional materials featuring strong anisotropy, which are of great relevance in potential spintronic and memory devices.

ASSOCIATED CONTENT

Supporting Information

The Supporting Information is available free of charge at https://pubs.acs.org/doi/10.1021/jacs.2c05894.

Synthesis of H_6HOTP species; experimental methods; theoretical framework and computational details; lattice geometry and crystal field; oxidation state of Co in the Co-HOTP network; calculations of spin quantum number; and calculation of the exchange interaction (J) (PDF)

AUTHOR INFORMATION

Corresponding Authors

Sofia O. Parreiras − *Instituto Madrileño de Estudios Avanzados en Nanociencia (IMDEA Nanoscience), E-28049 Madrid, Spain;* orcid.org/0000-0001-9009-1994; Email: sofia.oliveira@imdea.org

José I. Martínez − *Instituto de Ciencia de Materiales de Madrid (ICMM-CSIC), 28049 Madrid, Spain;* Email: joseignacio.martinez@icmm.csic.es

Carlos Martí-Gastaldo − *Instituto de Ciencia Molecular (ICMol), Universitat de València, 46980 Paterna, Spain;* orcid.org/0000-0003-3203-0047; Email: carlos.marti@uv.es

David Écija − *Instituto Madrileño de Estudios Avanzados en Nanociencia (IMDEA Nanoscience), E-28049 Madrid, Spain;* orcid.org/0000-0002-8661-8295; Email: david.ecija@imdea.org

Authors

Cristina Martín-Fuentes − *Instituto Madrileño de Estudios Avanzados en Nanociencia (IMDEA Nanoscience), E-28049 Madrid, Spain*

José I. Urgel − *Instituto Madrileño de Estudios Avanzados en Nanociencia (IMDEA Nanoscience), E-28049 Madrid, Spain;* orcid.org/0000-0001-7608-2979

Víctor Rubio-Giménez − *Instituto de Ciencia Molecular (ICMol), Universitat de València, 46980 Paterna, Spain;* Present Address: Centre for Membrane Separations, Adsorption, Catalysis, and Spectroscopy (cMACS), KU Leuven, Celestijnenlaan 200F, 3001 Leuven, Belgium; orcid.org/0000-0003-1269-5885

Beatriz Muñiz Cano − *Instituto Madrileño de Estudios Avanzados en Nanociencia (IMDEA Nanoscience), E-28049 Madrid, Spain*

Daniel Moreno − *Instituto Madrileño de Estudios Avanzados en Nanociencia (IMDEA Nanoscience), E-28049 Madrid, Spain*

Koen Lauwaet − *Instituto Madrileño de Estudios Avanzados en Nanociencia (IMDEA Nanoscience), E-28049 Madrid, Spain*

Manuel Valvidares − *ALBA Synchrotron Light Source, E-08290 Barcelona, Spain;* orcid.org/0000-0003-4895-8114

Miguel A. Valbuena − *Instituto Madrileño de Estudios Avanzados en Nanociencia (IMDEA Nanoscience), E-28049 Madrid, Spain;* orcid.org/0000-0002-0585-5636

Pierluigi Gargiani − *ALBA Synchrotron Light Source, E-08290 Barcelona, Spain;* orcid.org/0000-0002-6649-0538

Wolfgang Kuch − *Institut für Experimentalphysik, Freie Universität Berlin, 14195 Berlin, Germany;* orcid.org/0000-0002-5764-4574

Julio Camarero − *Instituto Madrileño de Estudios Avanzados en Nanociencia (IMDEA Nanoscience), E-28049 Madrid, Spain; Departamento de Física de la Materia Condensada and Condensed Matter Physics Center (IFIMAC), Universidad Autónoma de Madrid, 28049 Madrid, Spain;* orcid.org/0000-0003-0078-7280

José M. Gallego − *Instituto de Ciencia de Materiales de Madrid (ICMM-CSIC), 28049 Madrid, Spain*

Rodolfo Miranda − *Instituto Madrileño de Estudios Avanzados en Nanociencia (IMDEA Nanoscience), E-28049 Madrid, Spain; Departamento de Física de la Materia Condensada and Condensed Matter Physics Center (IFIMAC), Universidad Autónoma de Madrid, 28049 Madrid, Spain*

Complete contact information is available at: https://pubs.acs.org/10.1021/jacs.2c05894

Author Contributions

○C.M.-F. and S.O.P. contributed equally. The manuscript was written through contributions of all authors. All authors have given approval to the final version of the manuscript.

Notes

The authors declare no competing financial interest.

■ ACKNOWLEDGMENTS

This project has received funding from the European Research Council (ERC, grant 766555) and Marie Sklodowska-Curie Actions (MSCA, project 894924) under the European Union's Horizon 2020 research and innovation program, from Spanish MINECO (MAT2017-85089-C2-1-R, PID2019-108532GB-I00, and PID2020-118117RB-I00), from Comunidad Autónoma de Madrid via "Programa de Investigación Tecnologías" 2018 (FOTOART-CM S2018/NMT-4367, NANOMAG-COST-CM S2018/NMT-4321), and the Generalitat Valenciana (PROMETEU/2021/054). IMDEA Nanociencia and ICMol acknowledge support from the "Severo Ochoa" and "María de Maeztu" Programs for Centers of Excellence in R&D (MINECO, Grant SEV-2016-0686 and CEX2019-000919-M). The ALBA synchrotron is acknowledged for providing beam time at the BOREAS beamline (proposal number 2020094657).

■ REFERENCES

(1) Guirado-López, R. A.; Dorantes-Dávila, J.; Pastor, G. M. Orbital Magnetism in Transition-Metal Clusters: From Hund's Rules to Bulk Quenching. *Phys. Rev. Lett.* **2003**, *90*, No. 226402.
(2) Gambardella, P.; Rusponi, S.; Veronese, M.; Dhesi, S. S.; Grazioli, C.; Dallmeyer, A.; Cabria, I.; Zeller, R.; et al. Giant Magnetic Anisotropy of Single Cobalt Atoms and Nanoparticles. *Science* **2003**, *300*, 1130−1133.
(3) Autès, G.; Barreteau, C.; Spanjaard, D.; Desjonqueres, M.-C. Magnetism of iron: from the bulk to the monoatomic wire. *J. Phys.: Condens. Matter* **2006**, *18*, 6785−6813.
(4) Zadrozny, J. M.; Xiao, D. J.; Atanasov, M.; Long, G. J.; Grandjean, F.; Neese, F.; Long, J. R. Magnetic blocking in a linear iron(I) complex. *Nat. Chem.* **2013**, *5*, 577−581.
(5) Langenberg, A.; Hirsch, K.; Ławicki, A.; Zamudio-Bayer, V.; Niemeyer, M.; Chmiela, P.; Langbehn, B.; Terasaki, A.; Issendorff, B. V.; Lau, J. T. Spin and orbital magnetic moments of size-selected iron, cobalt, and nickel clusters. *Phys. Rev. B* **2014**, *90*, No. 184420.
(6) Rau, I. G.; Baumann, S.; Rusponi, S.; Donati, F.; Stepanow, S.; Gragnaniello, L.; Dreiser, J.; Piamonteze, C.; Nolting, F.; Gangopadhyay, S.; Albertini, O. R.; Macfarlane, R. M.; Lutz, C. P.; Jones, B. A.; Gambardella, P.; Heinrich, A. J.; Brune, H. Reaching the magnetic anisotropy limit of a 3d metal atom. *Science* **2014**, *344*, 988−992.
(7) Bunting, P. C.; Atanasov, M.; Damgaard-Møller, E.; Perfetti, M.; Crassee, I.; Orlita, M.; Overgaard, J.; van Slageren, J.; Neese, F.; Long, J. R. A linear cobalt(II) complex with maximal orbital angular momentum from a non-Aufbau ground state. *Science* **2018**, *362*, No. eaat7319.
(8) Jungwirth, T.; Marti, X.; Wadley, P.; Wunderlich, J. Antiferromagnetic spintronics. *Nat. Nanotechnol.* **2016**, *11*, 231−241.
(9) Baltz, V.; Manchon, A.; Tsoi, M.; Moriyama, T.; Ono, T.; Tserkovnyak, Y. Antiferromagnetic spintronics. *Rev. Mod. Phys.* **2018**, *90*, No. 015005.
(10) Gambardella, P.; Stepanow, S.; Dmitriev, A.; Honolka, J.; de Groot, F. M. F.; Lingenfelder, M.; Gupta, S. S.; Sarma, D. D.; Bencok, P.; Stanescu, S.; Clair, S.; Pons, S.; Lin, N.; Seitsonen, A. P.; Brune, H.; Barth, J. V.; Kern, K. Supramolecular control of the magnetic anisotropy in two-dimensional high-spin Fe arrays at a metal interface. *Nat. Mater.* **2009**, *8*, 189−193.
(11) Abdurakhmanova, N.; Tseng, T.-C.; Langner, A.; Kley, C. S.; Sessi, V.; Stepanow, S.; Kern, K. Superexchange-Mediated Ferromagnetic Coupling in Two-Dimensional Ni-TCNQ Networks on Metal Surfaces. *Phys. Rev. Lett.* **2013**, *110*, No. 027202.
(12) Faraggi, M. N.; Golovach, V. N.; Stepanow, S.; Tseng, T.-C.; Abdurakhmanova, N.; Kley, C. S.; Langner, A.; Sessi, V.; Kern, K.; Arnau, A. Modeling Ferro- and Antiferromagnetic Interactions in Metal−Organic Coordination Networks. *J. Phys. Chem. C* **2015**, *119*, 547−555.
(13) Xing, J.; Wang, P.; Jiang, Z.; Jiang, X.; Wang, Y.; Zhao, J. Rational design of 2D organic magnets with giant magnetic anisotropy based on two-coordinate 5d transition metals. *APL Mater.* **2020**, *8*, No. 071105.
(14) Wang, P.; Jiang, X.; Hu, J.; Zhao, J. Chemically Engineering Magnetic Anisotropy of 2D Metalloporphyrin. *Adv. Sci.* **2017**, *4*, No. 1700019.
(15) Wang, P.; Jiang, X.; Hu, J.; Huang, X.; Zhao, J. Giant magnetic anisotropy of a 5d transition metal decorated two-dimensional polyphthalocyanine framework. *J. Mater. Chem. C* **2016**, *4*, 2147−2154.
(16) Wang, P.; Jiang, X.; Hu, J.; Wang, B.; Zhou, T.; Yuan, H.; Zhao, J. Robust spin manipulation in 2D organometallic Kagome lattices: a first-principles study. *Phys. Chem. Chem. Phys.* **2020**, *22*, 11045−11052.
(17) Furukawa, H.; Cordova, K. E.; O' Keeffe, M.; Yaghi, O. M. The chemistry and applications of metal-organic frameworks. *Science* **2013**, *341*, No. 1230444.
(18) Cadiau, A.; Adil, K.; Bhatt, P. M.; Belmabkhout, Y.; Eddaoudi, M. A metal-organic framework−based splitter for separating propylene from propane. *Science* **2016**, *353*, 137−140.
(19) Kim, E. J.; Siegelman, R. L.; Jiang, H. Z. H.; Forse, A. C.; Lee, J.-H.; Martell, J. D.; Milner, P. J.; Falkowski, J. M.; Neaton, J. B.; Reimer, J. A.; Weston, S. C.; Long, J. R. Cooperative carbon capture and steam regeneration with tetraamine-appended metal−organic frameworks. *Science* **2020**, *369*, 392−396.
(20) Karmakar, A.; Samanta, P.; Desai, A. V.; Ghosh, S. K. Guest-Responsive Metal−Organic Frameworks as Scaffolds for Separation and Sensing Applications. Accounts of Chemical Research. *Acc. Chem. Res.* **2017**, *50*, 2457−2469.
(21) Bavykina, A.; Kolobov, N.; Khan, I. S.; Bau, J. A.; Ramirez, A.; Gascon, J. Metal-Organic Frameworks in Heterogeneous Catalysis: Recent Progress, New Trends, and Future Perspectives. *Chem. Rev.* **2020**, *120*, 8468−8535.
(22) Espallargas, G. M.; Coronado, E. Magnetic functionalities in MOFs: from the framework to the pore. *Chem. Soc. Rev.* **2018**, *47*, 533−557.
(23) Lin, Z.-J.; Lü, J.; Hong, M.; Cao, R. Metal−organic frameworks based on flexible ligands (FL-MOFs): structures and applications. *Chem. Soc. Rev.* **2014**, *43*, 5867−5895.
(24) Wang, M.; Dong, R.; Feng, X. Two-dimensional conjugated metal−organic frameworks (2D c-MOFs): chemistry and function for MOFtronics. *Chem. Soc. Rev.* **2021**, *50*, 2764−2793.
(25) Ko, M.; Mendecki, L.; Mirica, K. A. Conductive two-dimensional metal−organic frameworks as multifunctional materials. *Chem. Commun.* **2018**, *54*, 7873−7891.
(26) Xie, L. S.; Skorupskii, G.; Dincă, M. Electrically Conductive Metal−Organic Frameworks. *Chem. Rev.* **2020**, *120*, 8536−8580.
(27) Huang, X.; Zhang, S.; Liu, L.; Yu, L.; Chen, G.; Xu, W.; Zhu, D. Superconductivity in a Copper(II)-Based Coordination Polymer with Perfect Kagome Structure. *Angew. Chem., Int. Ed.* **2018**, *57*, 146−150.
(28) Zhang, X.; Zhou, Y.; Cui, B.; Zhao, M.; Liu, F. Theoretical Discovery of a Superconducting Two-Dimensional Metal−Organic Framework. *Nano Lett.* **2017**, *17*, 6166−6170.
(29) Dong, L.; Kim, Y.; Er, D.; Rappe, A. M.; Shenoy, V. B. Two-Dimensional π-Conjugated Covalent-Organic Frameworks as Quantum Anomalous Hall Topological Insulators. *Phys. Rev. Lett.* **2016**, *116*, No. 096601.
(30) Yamada, M. G.; Soejima, T.; Tsuji, N.; Hirai, D.; Dincă, M.; Aoki, H. First-principles design of a half-filled flat band of the kagome lattice in two-dimensional metal-organic frameworks. *Phys. Rev. B* **2016**, *94*, No. 081102.
(31) Hua, M.; Xia, B.; Wang, M.; Li, E.; Liu, J.; Wu, T.; Wang, Y.; Li, R.; Ding, H.; Hu, J.; Wang, Y.; Zhu, J.; Xu, H.; Zhao, W.; Lin, N. Highly Degenerate Ground States in a Frustrated Antiferromagnetic Kagome Lattice in a Two-Dimensional Metal−Organic Framework. *J. Phys. Chem. Lett.* **2021**, *12*, 3733−3739.
(32) Barth, J. V. Fresh perspectives for surface coordination chemistry. *Surf. Sci.* **2009**, *603*, 1533−1541.

(33) Dong, L.; Gao, Z.; Lin, N. Self-assembly of metal−organic coordination structures on surfaces. *Prog. Surf. Sci.* **2016**, *91*, 101−135.
(34) Liu, J.; Abel, M.; Lin, N. On-Surface Synthesis: A New Route Realizing Single-Layer Conjugated Metal−Organic Structures. *J. Phys. Chem. Lett.* **2022**, *13*, 1356−1365.
(35) Zhang, R.; Liu, J.; Gao, Y.; Hua, M.; Xia, B.; Knecht, P.; Papageorgiou, A. C.; Reichert, J.; Barth, J. V.; Xu, H.; Huang, L.; Lin, N. On-surface Synthesis of a Semiconducting 2D Metal−Organic Framework Cu3(C6O6) Exhibiting Dispersive Electronic Bands. *Angew. Chem., Int. Ed.* **2020**, *59*, 2669−2673.
(36) Meng, X.; Kolodzeiski, E.; Huang, X.; Timmer, A.; Lammers, B. S.; Gao, H.-Y.; Mönig, H.; Liu, L.; Xu, W.; Amirjalayer, S.; Zhu, D.; Fuchs, H. Tunable Thiolate Coordination Networks on Metal Surfaces. *ChemNanoMat* **2020**, *6*, 1479−1484.
(37) Lischka, M.; Dong, R.; Wang, M.; Martsinovich, N.; Fritton, M.; Grossmann, L.; Heckl, W. M.; Feng, X.; Lackinger, M. Competitive Metal Coordination of Hexaaminotriphenylene on Cu(111) by Intrinsic Copper Versus Extrinsic Nickel Adatoms. *Chem. - Eur. J.* **2019**, *25*, 1975−1983.
(38) Hmadeh, M.; Lu, Z.; Liu, Z.; Gándara, F.; Furukawa, H.; Wan, S.; Augustyn, V.; Chang, R.; Liao, L.; Zhou, F.; Perre, E.; Ozolins, V.; Suenaga, K.; Duan, X.; Dunn, B.; Yamamto, Y.; Terasaki, O.; Yaghi, O. M. New Porous Crystals of Extended Metal-Catecholates. *Chem. Mater.* **2012**, *24*, 3511−3513.
(39) Rochefort, A.; Vernisse, L.; Gómez-Herrero, A. C.; Sánchez-Sánchez, C.; Martín-Gago, J. A.; Chérioux, F.; Clair, S.; Coraux, J.; Martínez, J. I. Role of the Structure and Reactivity of Cu and Ag Surfaces in the Formation of a 2D Metal−Hexahydroxytriphenylene Network. *J. Phys. Chem. C* **2021**, *125*, 17333−17341.
(40) Gómez-Herrero, A. C.; Sánchez-Sánchez, C.; Chérioux, F.; Martínez, J. I.; Abad, J.; Floreano, L.; Verdini, A.; Cossaro, A.; Mazaleyrat, E.; Guisset, V.; David, P.; Lisi, S.; Gago, J. A. M.; Coraux, J. Copper-assisted oxidation of catechols into quinone derivatives. *Chem. Sci.* **2021**, *12*, 2257−2267.
(41) Marele, A. C.; Corral, I.; Sanz, P.; Mas-Ballesté, R.; Zamora, F.; Yáñez, M.; Gómez-Rodríguez, J. M. Some Pictures of Alcoholic Dancing: From Simple to Complex Hydrogen-Bonded Networks Based on Polyalcohols. *J. Phys. Chem. C* **2013**, *117*, 4680−4690.
(42) Capdevila-Cortada, M.; Łodziana, Z.; López, N. Performance of DFT+U Approaches in the Study of Catalytic Materials. *ACS Catal.* **2016**, *6*, 8370−8379.
(43) Mähringer, A.; Jakowetz, A. C.; Rotter, J. M.; Bohn, B. J.; Stolarczyk, J. K.; Feldmann, J.; Bein, T.; Medina, D. D. Oriented Thin Films of Electroactive Triphenylene Catecholate-Based Two-Dimensional Metal−Organic Frameworks. *ACS Nano* **2019**, *13*, 6711−6719.
(44) Hollmann, N.; Hu, Z.; Valldor, M.; Maignan, A.; Tanaka, A.; Hsieh, H. H.; Lin, H.-J.; Chen, C. T.; Tjeng, L. H. Electronic and magnetic properties of the kagome systems $YBaCo_4O_7$ and $YBaCo_3MO_7$ (M = Al, Fe). *Phys. Rev. B.* **2009**, *80*, No. 085111.
(45) Hu, Z.; Wu, H.; Haverkort, M. W.; Hsieh, H. H.; Lin, H. -J.; Lorenz, T.; Baier, J.; Reichl, A.; Bonn, I.; Felser, C.; Tanaka, A.; Chen, C. T.; Tjeng, L. H. Different Look at the Spin State of Co^{3+} Ions in a CoO_5 Pyramidal Coordination. *Phys. Rev. Lett.* **2004**, *92*, No. 207402.
(46) Mandziak, A.; Soria, G. D.; Prieto, J. E.; Prieto, P.; Granados-Miralles, C.; Quesada, A.; Foerster, M.; Aballe, L.; de la Figuera, J. Tuning the Néel temperature in an antiferromagnet: the case of $Ni_xCo_{1-x}O$ microstructures. *Sci. Rep.* **2019**, *9*, No. 13584.
(47) Singh, V. R.; Sakamoto, Y.; Kataoka, T.; Kobayashi, M.; Yamazaki, Y.; Fujimori, A.; Chang, F.-H.; Huang, D.-J.; Lin, H.-J.; Chen, C. T.; Toyosaki, H.; Fukumura, T.; Kawasaki, M. Bulk and surface magnetization of Co atoms in rutile $Ti_{1-x}Co_xO_{2-\delta}$ thin films revealed by x-ray magnetic circular dichroism. *J. Phys.: Condens. Matter.* **2011**, *23*, No. 176001.
(48) Thole, B. T.; Carra, P.; Sette, F.; van der Laan, G. X-ray circular dichroism as a probe of orbital magnetization. *Phys. Rev. Lett.* **1992**, *68*, 1943−1946.
(49) Carra, P.; Thole, B. T.; Altarelli, M.; Wang, X. X-ray circular dichroism and local magnetic fields. *Phys. Rev. Lett.* **1993**, *70*, 694−697.
(50) Hermanns, C. F.; Bernien, M.; Krüger, A.; Walter, W.; Chang, Y.-M.; Weschke, E.; Kuch, W. Huge magnetically coupled orbital moments of Co porphyrin molecules and their control by CO adsorption. *Phys. Rev. B* **2013**, *88*, No. 104420.
(51) Gambardella, P.; Dhesi, S. S.; Gardonio, S.; Grazioli, C.; Ohresser, P.; Carbone, C. Localized Magnetic States of Fe, Co, and Ni Impurities on Alkali Metal Films. *Phys. Rev. Lett.* **2002**, *88*, No. 047202.

https://doi.org/10.1021/jacs.2c05894
J. Am. Chem. Soc. 2022, 144, 16034−16041